

Diffraction Analysis of LC Gratings based on Linearly Graded Phase Model for Surface Anchoring Energies

Chang-Jae Yu*[a] and Sin-Doo Lee*[b]

Abstract

We reported the diffraction analysis of the liquid crystal (LC) binary gratings and the surface anchoring energies for planar and homeotropic alignments. The planar and homeotropic anchoring energies were directly derived based on the linearly distorted director distribution near domain boundaries, in which the distorted lengths correspond to the extrapolation lengths into both planar and homeotropic regions. From the diffraction analysis for the LC binary gratings with various grating periods based on the linearly graded phase model, both distorted lengths into planar and homeotropic regions were simultaneously obtained. In this work, the planar and homeotropic anchoring energies were found to be about 1.4×10^{-4} J/m^2 and 0.9×10^{-5} J/m^2, respectively.

Keywords : liquid crystal, diffraction grating, anchoring energy, photoalignment

1. Introduction

Liquid crystals (LCs) are very useful in several key areas of flat panel displays and optical devices. Moreover, the multi-ordered LC systems have attracted great interest and have been widely studied because of the importance of fundamental research in low dimensional phenomena and their potential for device applications to the optical systems including displays. As one of the device structures with multi-ordered interfaces, the binary grating configurations play an important role in various optical systems and three-dimensional (3D) displays [1-4]. In the binary gratings, their diffraction properties show anomalous behavior due to the distortion of the LC director at domain boundaries, which are directly governed by surface anchoring energies [5]. For the fundamental researches as well as device applications, the surface anchoring energy is one of the important factors for characterizing the surface orientation of the LC molecules and the electrooptic (EO) properties of the LC devices.

A variety of techniques such as the wedge-cell method [6,7], the external field method [8,9], and the fully leaky waveguide method [10,11] have been employed for measuring the polar anchoring energy. With the help of the external field, the homogenous (planar) anchoring energy was measured for the LCs with positive dielectric anisotropy while the homeotropic one for the LCs with negative dielectric anisotropy.

In this work, we report in detail about the diffraction properties of the LC gratings based on the linearly graded phase (LGP) model [12] and the surface anchoring energies for planar and homeotropic alignments based on the linearly distorted director (LDD) approximation [13]. Using this method, both planar and homeotropic surface anchoring energies of the LCs were simultaneously measured by optical diffraction in the binary grating.

Manuscript received August 18, 2007; accepted for publication September 15, 2007.
This work was supported in part by Korea Research Foundation Grant (KRF-2004-005-D00165).
* Member, KIDS
Corresponding Author : Chang-Jae Yu
[a]Department of Electronics and Computer Engineering, Hanyang University, Seoul 133-791, Korea.
[b]School of Electrical Engineering, Seoul National University, Seoul 151-742, Korea
E-mail : cjyu@hanyang.ac.kr **Tel** : 02-2220-2314

2. Linearly distorted director approximation

In the LC binary grating as shown in Fig. 1, the surface anchoring energies of the LCs in both planar and homeotropic domains influence significantly the diffraction patterns of the LC binary grating. Fig. 2 shows the molecular tilt angle of the LC director near the domain boundary between the homeotropic and hybrid domains.

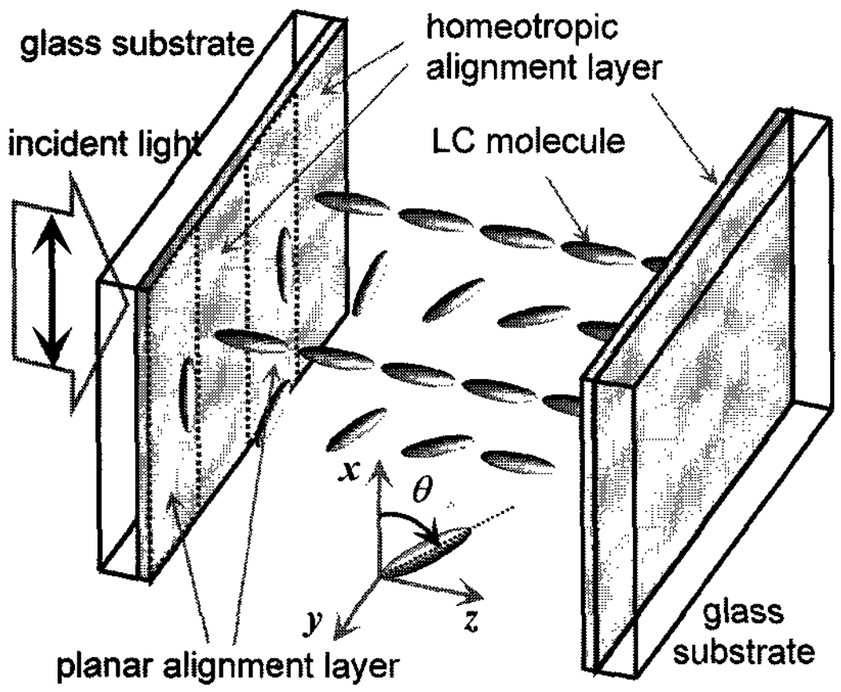

Fig. 1. The LC binary grating structure consisting of periodic striped domains in an alternating the homeotropic and hybrid geometry.

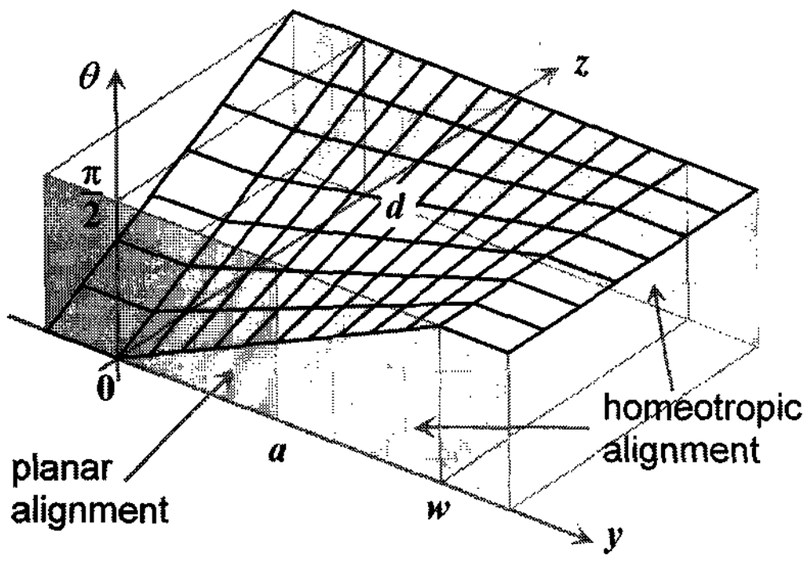

Fig. 2. The distributions of the molecular tilt angle of the LC director proposed in the LDD approximation near the domain boundary between the homeotropic and hybrid domains.

According to the continuum theory [14], the LC director profile was numerically obtained, from the minimization of the total free energy consisting of the elastic deformation energy and the surface anchoring energy.

For simplification, we assumed that the LC directors were linearly distorted into homeotropic and hybrid regions along the y-axis and into bulk along the z-axis near domain boundary. Under these assumptions, the distribution of the tilt angle θ of the LC director near the domain boundary is shown in Fig. 2. On the top substrate at $z = 0$, the planar alignment was produced in the region of $0 \le y \le a$ and the homeotropic one in the region of $a \le y \le w$. On the bottom substrate at $z = d$, the homeotropic alignment layer was prepared. Here, the regions of $y < 0$ and $y > w$ correspond to the intrinsically hybrid and homeotropic domains, respectively. As a result, the LC director was linearly twisted along the y-axis in the range of $a \le y \le w$ because of the curvature elasticity [14]. As shown in Fig. 2, the tilt angle θ of the LC director on the yz-plane is expressed as

$$\theta(y,z) = \frac{\pi}{2} - \frac{\pi}{2wd}(w-y)(d-z), \tag{1}$$

where d represents the cell thickness.

In this linearly deformed director (LDD) approximation, the phase profile in the LC grating configuration was obtained by the 2 × 2 Jones matrix method [15]. Fig. 3(a) shows the phase profile of the LC grating, obtained by 2 × 2 Jones matrix method, corresponding to the director distribution shown in Fig. 2. Here, the dotted line and the dashed line represent the corresponding phase profile based on the elastic continuum model and those based on the LDD approximation [12], respectively. The solid line describes a linearly graded phase (LGP) profile, which is approximated to be straight line between two relative phases. The intensities for each diffraction order for these cases werecalculated by the discrete Fourier transformation

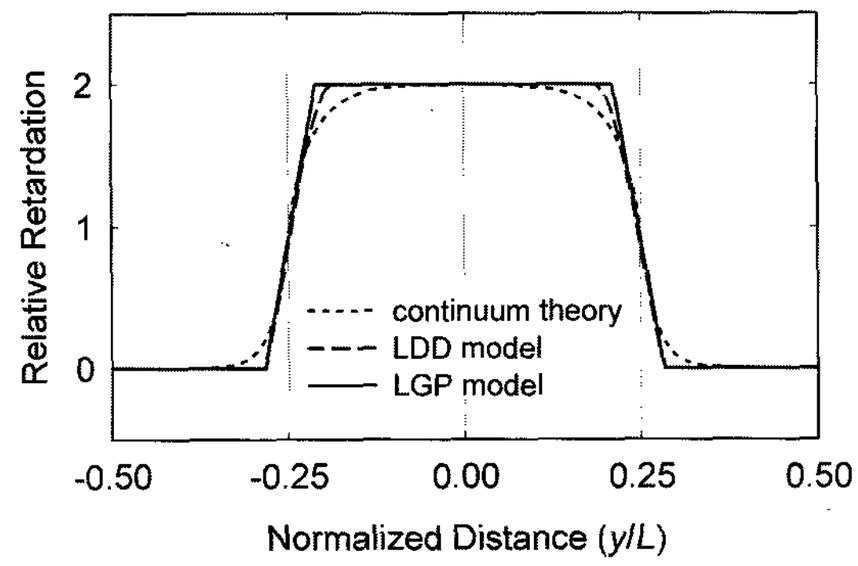

Fig. 3. (a) The phase profiles of the LC binary grating evaluated from the elastic continuum theory, the LDD approximation, and the simple LGP model. (b) The intensities for each diffraction order calculated by the discrete Fourier transformation for the corresponding phase profiles.

[16] of the phase profile and are denoted as open symbols in Fig. 3(b). It should be noted that the diffraction results in the three models are in excellent agreement with each other.

We now discuss the total free energy with the LC director distribution shown in Eq. (1). Using the Rapini-Papoular anchoring energy [17], the total free energy without an external electric field within the distorted region on the *yz*-plane is described as

$$F_{tot} = \frac{\pi^2 K_{eff}}{24wd}\left(d^2+w^2\right)-\frac{w}{4\pi}\left(W_p+W_h\right)\sin\left(\frac{a\pi}{w}\right) + \frac{1}{4}\left[wW_h+a\left(W_p-W_h\right)\right], \tag{2}$$

where K_{eff}, W_{p}, and W_{h} are the relevant elastic constant, the planar anchoring strength, and the homeotropic anchoring strength, respectively. Minimizing Eq. (2) with respect to a, the length a is readily obtained as

$$\frac{a}{w}=\frac{1}{\pi}\cos^{-1}\left(\frac{1-\zeta}{1+\zeta}\right), \tag{3}$$

where $\zeta = W_{\text{h}}/W_{\text{p}}$. Note that a approaches w ($a/w \to 1$) for $\zeta >> 1$ ($W_{\text{h}} >> W_{\text{p}}$) and approaches zero ($a/w \to 0$) for $\zeta << 1$ ($W_{\text{h}} << W_{\text{p}}$). When $W_{\text{h}} = W_{\text{p}}$ ($\zeta = 1$), the ratio of distorted lengths become to be 1/2 ($a/w = 0.5$). Substituting Eq. (3) into Eq. (2), the total free energy F_{tot} can be written in terms of w. Finally, the minimization of Eq. (2) with respect to w gives the width w as

$$w = d\left[1+\frac{6d}{\pi^3 K_{eff}}W_p\Xi(\zeta)\right]^{-\frac{1}{2}}, \tag{4}$$

where

$$\Xi(\zeta)=\pi\zeta-2\sqrt{\zeta}+(1+\zeta)\cos^{-1}\left(\frac{1-\zeta}{1+\zeta}\right). \tag{5}$$

Using the lengths, a and w, which were measured experimentally in the configuration as shown in Fig. 1, the parameter ζ can be obtained from Eq. (3). Accordingly, the extrapolation length, $K_{\text{eff}}/W_{\text{p}}$, for the planar case can be determined from Eqs. (4) and (5), while $K_{\text{eff}}/W_{\text{h}}$ for the homeotropic case can be obtained from the parameter ζ. Note that the two extrapolation lengths are directly related to the corresponding surface anchoring energies.

For a given distorted length w, the extrapolation length associated with the planar anchoring energy increases with increasing ratio of the distorted length, a/w, while the corresponding anchoring energy (planar anchoring energy) decreases. This means that a small anchoring energy allows distortion to penetrate into its own alignment domain. In principle, the LC molecules on the surface with an infinite anchoring energy are fixed along the aligning direction with no distortion near domain boundary. By increasing the whole distortion length, the extrapolation length increases, while the anchoring energy decreases.

3. Linearly graded phase model in LC diffraction

We now introduce the optical diffraction formula within a LGP profile in the LC binary grating to determine the distorted lengths, a and w [12] since the phase profile corresponding to the LDD approximation is in excellent agreement with the phase profile for the LGP model as shown in Fig. 3. Fig. 4 shows the LGP profile corresponding to the LDD approximation. A whole distorted length and distorted lengths penetrated into the planar alignment region and the homeotropic alignment region are denoted by w, a, and b, respectively.

Let us now analytically describe the diffraction properties of the above LC binary grating device. In Fig. 4, the amplitude transmittance function of the LC grating devices is expressed as,

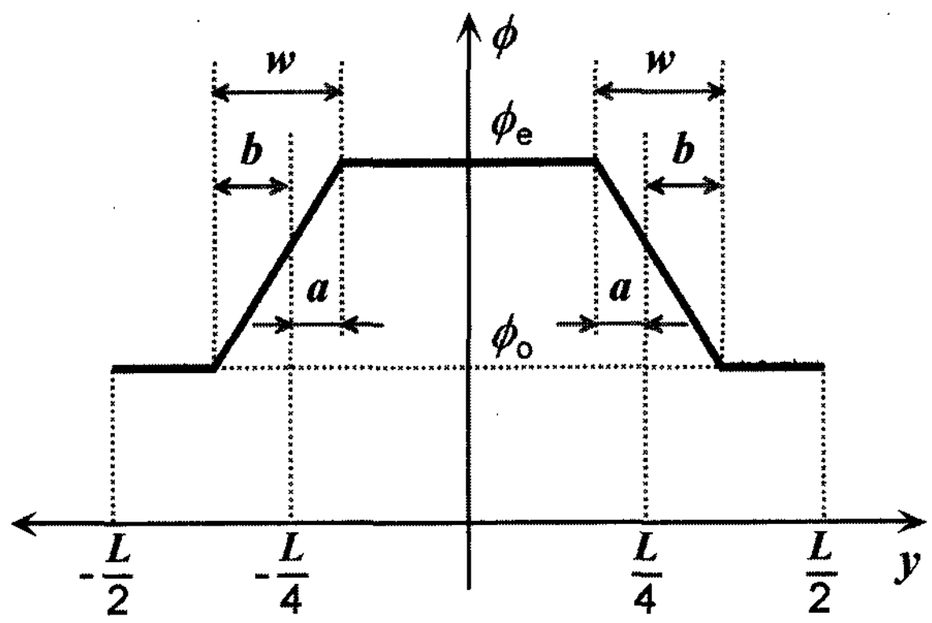

Fig. 4. The simple LGP profile corresponding to the LDD approximation. The values a/L and b/L, scaled by the grating period, directly correspond to the distortion lengths in the LGP model.

$$t_A(y)=\begin{cases}\exp[i\phi_o] & -\frac{1}{2}\le\frac{y}{L}\le-\frac{1}{4}-\xi_2\\ \exp\left[i\left(\alpha\frac{y}{L}+\beta\right)\right] & -\frac{1}{4}-\xi_2\le\frac{y}{L}\le-\frac{1}{4}+\xi_1\\ \exp[i\phi_e] & -\frac{1}{4}+\xi_1\le\frac{y}{L}\le\frac{1}{4}-\xi_1\\ \exp\left[i\left(-\alpha\frac{y}{L}+\beta\right)\right] & \frac{1}{4}-\xi_1\le\frac{y}{L}\le\frac{1}{4}+\xi_2\\ \exp[i\phi_o] & \frac{1}{4}+\xi_2\le\frac{y}{L}\le\frac{1}{2}\end{cases} \quad (6)$$

where

$$\alpha = \frac{\phi_e-\phi_o}{\xi_1+\xi_2},$$
$$\beta = \frac{1}{4}\frac{\phi_e-\phi_o}{\xi_1+\xi_2}+\frac{\xi_2\phi_e+\xi_1\phi_o}{\xi_1+\xi_2}. \quad (7)$$

Here, the distorted parameters ξ_1 and ξ_2 directly correspond to the values a/L and b/L (scaled by the grating period L) in the LDD model in Fig. 2, respectively. The phases in the homeotropic region and the hybrid region are depicted by ϕ_o and ϕ_e, respectively.

Using the Fraunhofer diffraction formalism [18], the k-th order Fourier component c_k is expressed as

$$c_k=\frac{1}{L}\int_{-\frac{L}{2}}^{\frac{L}{2}} t_A(y)\exp\left(i\frac{2\pi k}{L}y\right)\,dy. \quad (8)$$

In the case of the unlimited size of the grating and beam spot, the diffraction efficiency of the k-th order is given as the absolute square of c_k in the first-order approximation [18]. As a result, the non-diffraction (zeroth order diffraction) efficiency, η_0 is expressed as

$$\eta_0=4\xi_-^2\sin^2\left(\frac{\Delta\phi}{2}\right)+\left[(1-2\xi_+)\cos\left(\frac{\Delta\phi}{2}\right)+2\xi_+\mathrm{sinc}\left(\frac{\Delta\phi}{2}\right)\right]^2, \quad (9)$$

where $\xi_\pm = \xi_1 \pm \xi_2$ and $\Delta\phi = \phi_e - \phi_o$. Similarly, the k-th order diffraction efficiency, η_k (k is a non-zero integer) is

$$\eta_k = \left(\xi_+\Phi_+-\frac{1}{\pi k}\Psi_-\right)^2\cos^2\left(\frac{\pi k}{2}+\pi k\xi_-\right) + \left(\xi_+\Phi_--\frac{1}{\pi k}\Psi_+\right)^2\sin^2\left(\frac{\pi k}{2}+\pi k\xi_-\right), \quad (10)$$

where

$$\Phi_\pm = \mathrm{sinc}\left(\frac{\Delta\phi}{2}+\pi k\xi_+\right)\pm\mathrm{sinc}\left(\frac{\Delta\phi}{2}-\pi k\xi_+\right),$$
$$\Psi_\pm = \sin\left(\frac{\Delta\phi}{2}+\pi k\xi_+\right)\pm\sin\left(\frac{\Delta\phi}{2}-\pi k\xi_+\right). \quad (11)$$

For $\xi_1 = \xi_2 = 0$ ($\xi_- = \xi_+ = 0$) corresponding to the case of the ideal binary grating [18] is simply expressed as

$$\eta_0^* = \cos^2\left(\frac{\Delta\phi}{2}\right). \quad (12)$$

Similarly, k-th order diffraction efficiency, η_k^* is

$$\eta_k^* = \sin^2\left(\frac{\Delta\phi}{2}\right)\mathrm{sinc}^2\left(\frac{\pi k}{2}\right). \quad (13)$$

Note that for the ideal binary grating, no diffraction occurs at even order positions irrespective of the phase difference $\Delta\phi$ from Eq. (13) since $\sin(\pi k/2) = 0$ when k is even number.

4. Experiments

The LC binary gratings with the periodic homeotropic and hybrid alignments were fabricated by glass substrates coated with the photopolymer of LGC-M1 (LG Cable Ltd., Korea) [19]. The photopolymer aligns the LC molecules homogeneously under the illumination of a linearly polarized ultraviolet (LPUV) light and homeotropically on a non-treated substrate with the LPUV light [12]. The alternating binary nature of the LC gratings was prepared with one-step exposure of a LPUV light through an amplitude photomask at 2.0 mW for 2 minutes. The pretilt angle was 3° in the UV exposed region while it was about 89° in the unexposed region. For a given cell thickness and surface conditions (planar and homeotropic surface anchoring energies), only the grating period L was varied using one photomask with different grating periods. The grating period varied from 19 μm to 300 μm with an equivalent duty between the homeotropic and hybrid domains.

The LC material used in this study was a nematic LC of MLC-6012 (E. Merck). The ordinary and extraordinary refractive indices of MLC-6012 are $n_o = 1.4620 + 5682/\lambda^2$ and $n_e = 1.5525 + 9523/\lambda^2$, respectively, where λ is the wavelength of the incident light in nanometers [20]. The cell thicknesses were maintained using glass spacers of 4.28 μm and 9.58 μm.

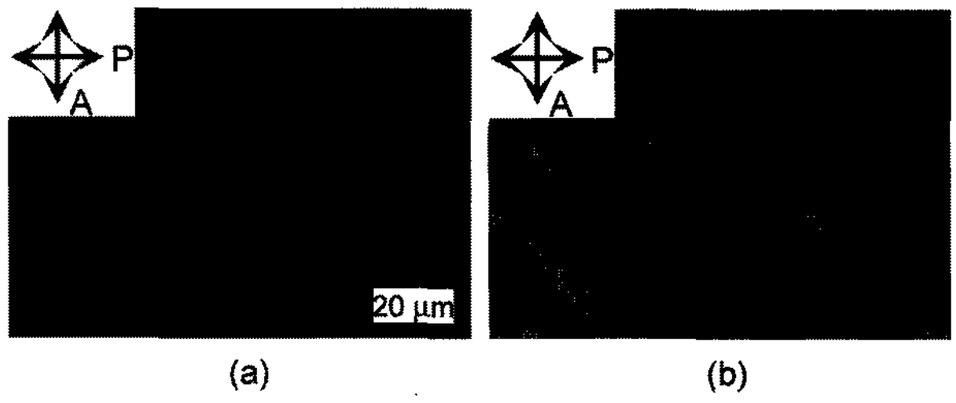

Fig. 5. Microscopic textures of our LC grating showing two alternating stripes observed at an angle of (a) 0° and (b) 45° between the grating vector and one of crossed polarizers.

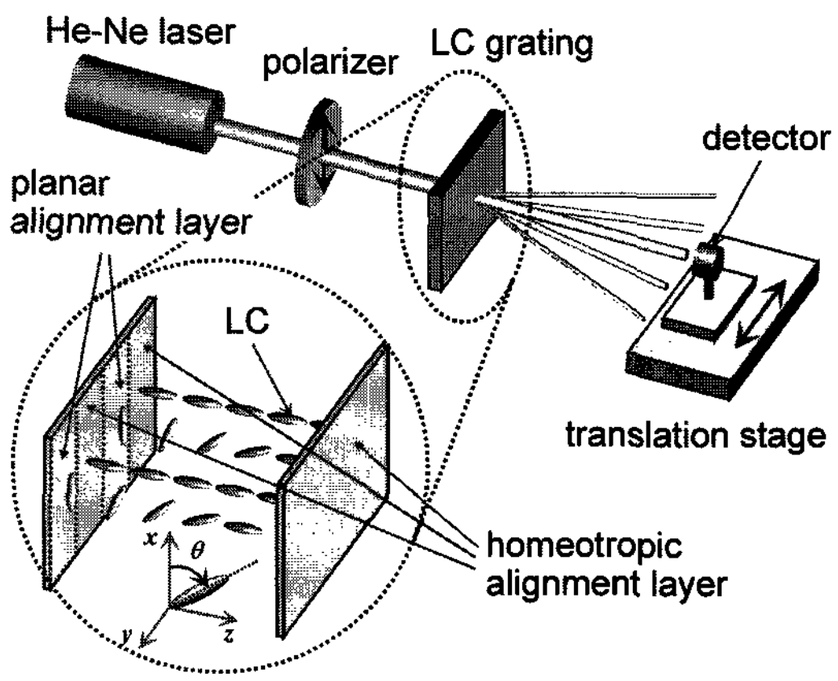

Fig. 6. The experimental setup for measuring the diffraction patterns of the LC gratings using a photodetector mounted on a motorized translation stage. The polarization state of incident light is perpendicular to the direction of the grating vector.

Microscopic textures of our LC binary gratings in periodic homeotropic and hybrid geometries are shown in Fig. 5. The photographs of Figs. 5(a) and 5(b) showing two alternating stripes were taken with a polarizing optical microscope (Nikon, Optiphotpol II) under crossed polarizers when the grating vector makes angles of 0° and 45° with respect to one of the crossed polarizers. In this case, the binary nature of the LC grating structure will be capable of spatially controlling the phase modulation and the polarization of an input beam by adjusting an applied voltage.

The polarization state of an incident light is parallel to the x-axis which is perpendicular to the direction of the grating vector (y-axis). The x-polarized light experiences the phase modulation as shown in Fig. 4. A He-Ne laser of 0.633 μm and a photodetector mounted on a motorized translation stage were used to measure the diffraction intensity profiles as shown in Fig. 6. All the measurements were carried out at room temperature.

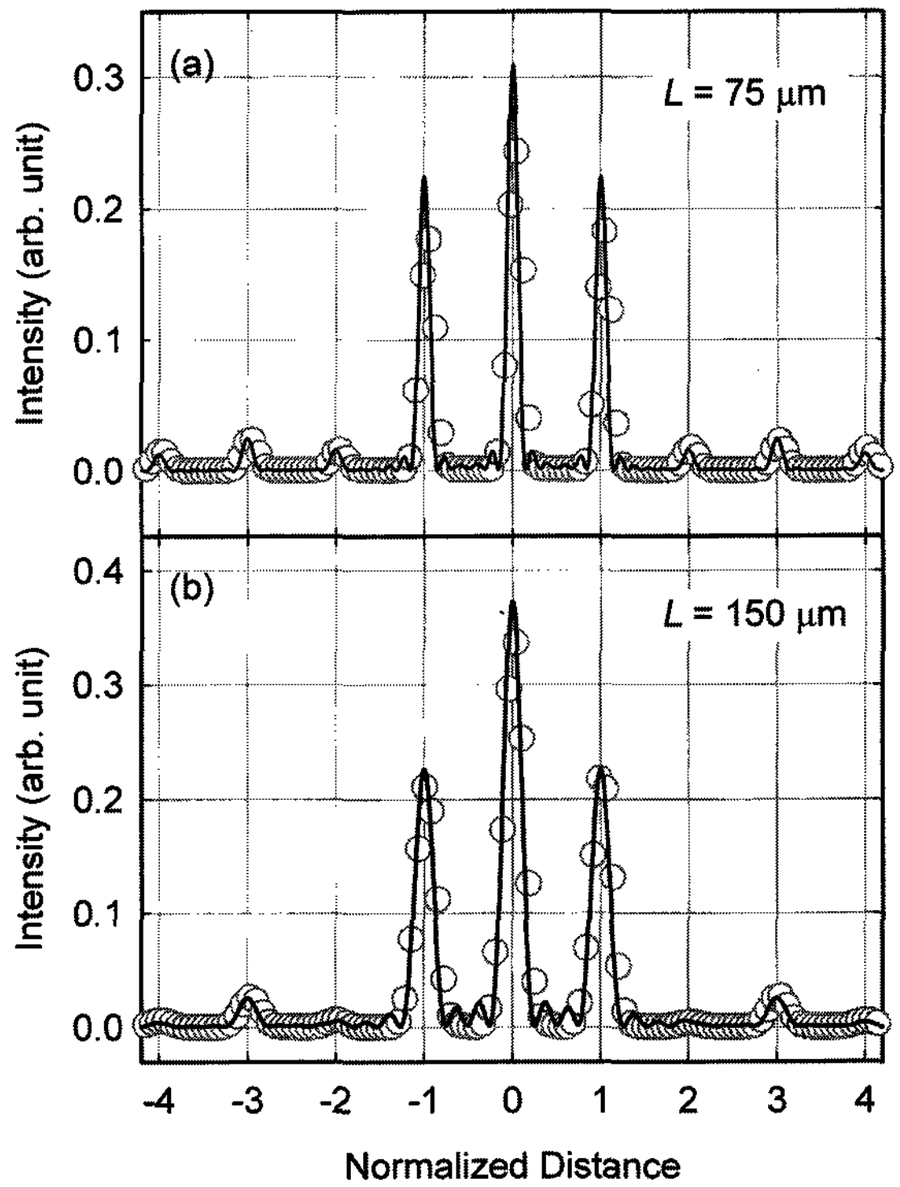

Fig. 7. The diffraction patterns of the LC binary grating as a function of the normalized distance with the grating periods of (a) L = 75 μm and (b) L = 150 μm for the cell thickness d = 9.58 μm at the wavelength of λ = 0.633 μm, respectively. Opened circles and solid lines represent the measured intensities and the calculated patterns, respectively.

5. Results and discussion

Fig. 7 shows the diffraction intensity profiles of the linearly graded LC binary gratings with various grating periods for the cell thickness of 9.58 μm. Here, the normalized distance represents the unit distance for each order of diffraction in the grating along the y-axis. Opened circles and solid lines represent the measured diffraction intensities and the theoretical results using the convolution theorem [18], Eqs. (9) and (10) directly evaluated from the LGP model, respectively.

For the LC grating with the cell thickness of d = 9.58 μm as shown in Fig. 7, the fitting parameters ξ_1 = 0.0485 and ξ_2 = 0.0088 were used for L = 75 μm and ξ_1 = 0.0243 and ξ_2 = 0.0043 for L = 150 μm. Note that all the even order diffractions vanish in an ideal binary grating as expressed in Eq. (13). For L = 75 μm in d = 9.58 μm in Fig. 7(a), finite but small diffraction intensities were observed at the even orders. This is attributed to the distortions of the LC director in the interfacial regions of ξ_1 and ξ_2 near the

domain boundaries. For L = 150 μm in d = 9.58 μm, on the other hand, the even order diffractions almost disappear as in an ideal binary grating. Thus, the distorted parameters ξ_1 and ξ_2, scaled by the grating period L, mainly govern the diffraction patterns of the LC binary gratings.

From the least-squares-fits of the diffraction data to Eqs. (9) and (10) using the convolution theorem [18], the parameters ξ_1 and ξ_2 are readily determined. As a consequence, the anchoring energies, W_p and W_h, can be obtained by substituting a and w into Eqs. (3)-(5).

For the different cell thicknesses, the parameters of ξ_1 and ξ_2, determined by fitting the experimental data to Eqs. (9) and (10), as a function of the inverse grating period ($1/L$) are shown in Fig. 8. For simulation, the experimental results shown in Fig. 7 were used for various grating periods varying from 19 μm to 300 μm. Here, the solid lines represent the least-squares-fits of the data to straight lines. As shown in Fig. 8, the parameters, ξ_1 and ξ_2, are inversely proportional to the grating period. Moreover, the slopes of the straight lines for ξ_1 and ξ_2 correspond to the actual distorted lengths, which in turn correspond to the extrapolation lengths, into the hybrid and homeotropic domains for each cell thickness, respectively.

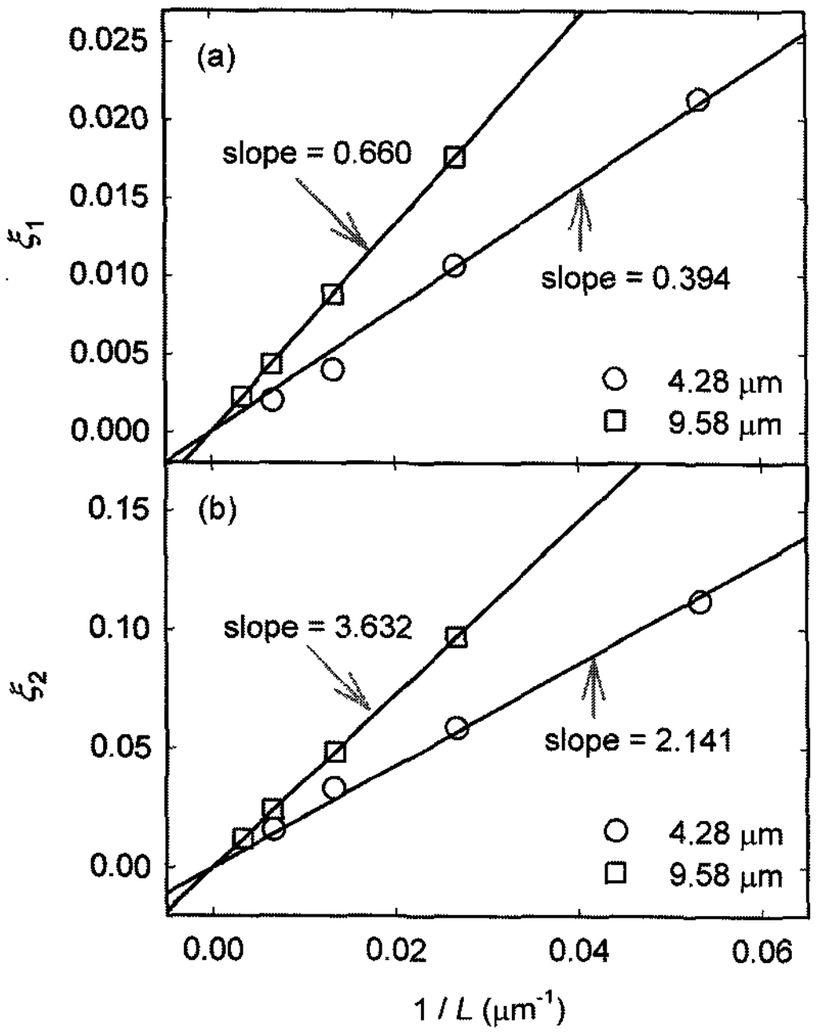

Fig. 8. The distortion parameters (a) ξ_1 and (b) ξ_2 as a function of $1/L$ for the cell thicknesses of d = 4.28 μm and d = 9.58 μm. Opened symbols were evaluated from the LGP model for various grating periods. Solid lines represent the least-squares-fits of the data to straight lines.

Table 1. The fitting results of the distortion parameters and the corresponding anchoring energies at the cell thicknesses of d = 4.28 μm and d = 9.58 μm.

parameters	d = 4.28 μm	d = 9.58 μm
$\xi_1 L$	0.394 μm	0.660 μm
$\xi_2 L$	2.141 μm	3.632 μm
W_p	$(1.44 \pm 0.18) \times 10^{-4}$ J/m^2	$(1.42 \pm 0.23) \times 10^{-4}$ J/m^2
W_h	$(8.86 \pm 0.57) \times 10^{-6}$ J/m^2	$(8.59 \pm 0.82) \times 10^{-6}$ J/m^2

The slopes corresponding to ξ_1 and ξ_2 were fitted to be 0.394 and 2.141 for d = 4.28 μm, and 0.660 and 3.632 for d = 9.58 μm, respectively. In fact, ξ_1 and ξ_2, representing the slopes the straight lines, are certain constants corresponding to the linearly distorted lengths at the interface of the two domains, irrespective of the grating period L. Thus, $\xi_1 L$ and $\xi_2 L$ become distorted lengths a and $b = (w-a)$ as in Fig. 4, respectively. From the fitting parameters, the anchoring strengths W_p and W_h were estimated to be $(1.44 \pm 0.18) \times 10^7$ K_{eff} J/Nm^2 and $(8.96 \pm 0.57) \times 10^5$ K_{eff} J/Nm^2 for d = 4.28 μm and $(1.42 \pm 0.23) \times 10^7$ K_{eff} J/Nm^2 and $(8.59 \pm 0.82) \times 10^5$ K_{eff} J/Nm^2 for d = 9.58 μm, respectively. With a typical value of the relevant elastic constant $K_{eff} \approx 10^{-11}$ N, the planar anchoring energy, W_p, is on the order of 10^{-4} J/m^2 and the homeotropic anchoring energy, W_h, is on the order of 10^{-5} J/m^2. The fitting results of the distorted parameters and the corresponding anchoring energies are summarized in Table 1.

6. Conclusions

We reported about the diffraction properties of the LC binary gratings and the surface anchoring energies for planar and homeotropic alignments. The LC binary gratings were prepared by the top substrate with periodic planar and homeotropic alignments and the bottom substrate with a homeotropic alignment for whole region. Based on the LDD model, the homeotropic and planar anchoring energies were directly derived from the distorted lengths, corresponding to the extrapolation lengths into both planar and homeotropic regions. Using the diffraction formula in the LPG model with the phase profile of a trapezoid, the actual distorted lengths were easily obtained from the diffraction analysis for the LC binary gratings with various grating periods. In

the frame of our work, the planar and homeotropic anchoring energies were found to be about 1.4×10^{-4} J/m^2 and 0.9×10^{-5} J/m^2, respectively. Since the anchoring energy strongly depends on an interaction between alignment layers and LC materials, the extensive investigation of the surface anchoring energies with various LC materials remains to be explored.

References

[1] E. Hasman, Z. Bomzon, A. Niv, G. Biener, and V. Kleiner, *Opt. Commun.* **209**, 45 (2002).

[2] J. A. Davis, J. Adachi, C. R. Fernández-Pousa, and I. Moreno, *Opt. Lett.* **26**, 587 (2001).

[3] M. Ivanov and T. Eiju, *Proc. SPIE* **4580**, 664 (2001).

[4] S. Jung, J.-H. Park, H. Choi, and B. Lee, *Appl. Opt.* **42**, 2513 (2003).

[5] H. Ono, S. Oikawa, and N. Kawatsuki, *J. Appl. Phys.* **101**, 123523 (2007).

[6] D. Riviere, Y. Levy, and E. Guyon, *J. Phys. (France) Lett.* **40**, L215 (1979).

[7] G. Barbero, N. V. Madhusudana, and G. Durand, *J. Phys. (France) Lett.* **45**, L613 (1984).

[8] K. H. Yang, *J. Appl. Phys.* **53**, 6742 (1982).

[9] H. Yokoyama and H. A. van Sprang, *J. Appl. Phys.* **57**, 4520 (1985).

[10] F. Yang, J. R. Sambles, Y. Dong, and H. Gao, *J. Appl. Phys.* **87**, 2726 (2000).

[11] F. Yang, L. Ruan, and J. R. Sambles, *J. Appl. Phys.* **88**, 6175 (2000).

[12] C.-J. Yu, J.-H. Park, J. Kim, M.-S. Jung, and S.-D. Lee, *Appl. Opt.* **43**, 1783 (2004).

[13] C.-J. Yu, J.-H. Park, and S.-D. Lee, *Appl. Surf. Sci.* **238**, 385 (2004).

[14] P. G. de Gennes and J. Prost, *The Physics of Liquid Crystals* (Oxford University Press, New York, 1993)

[15] P. Yeh, *Optical Waves in Layered Media* (John Wiley & Sons, Chichester, 1988).

[16] W. H. Press, B. P. Flannery, S. A. Teukolsky, and W. T. Vetterling, *Numerical Recipes : The Art of Scientific Computing* (Cambridge University Press, New York, 1986).

[17] A. Rapini and M. J. Papoular, *J. Phys. (Paris) Colloq.* **30**, C4-54 (1969).

[18] J. W. Goodman, *Introduction to Fourier Optics* (McGraw-Hill Book Co., Singapore, 1996).

[19] J.-H. Park, C.-J. Yu, J. Kim, S.-Y. Chung, and S.-D. Lee, *Appl. Phys. Lett.* **83**, 1918 (2003).

[20] Data provided by E. Merck Company.